scientific reports

Check for updates

OPEN

Large area MoS_2 thin film growth by direct sulfurization

Kai-Yao Yang[1], Hong-Thai Nguyen[2], Yu-Ming Tsao[2], Sofya B. Artemkina[3,4], Vladimir E. Fedorov[3,4], Chien-Wei Huang[1,5]✉ & Hsiang-Chen Wang[2,6]✉

In this study, we present the growth of monolayer MoS_2 (molybdenum disulfide) film. Mo (molybdenum) film was formed on a sapphire substrate through e-beam evaporation, and triangular MoS_2 film was grown by direct sulfurization. First, the growth of MoS_2 was observed under an optical microscope. The number of MoS_2 layers was analyzed by Raman spectrum, atomic force microscope (AFM), and photoluminescence spectroscopy (PL) measurement. Different sapphire substrate regions have different growth conditions of MoS_2. The growth of MoS_2 is optimized by controlling the amount and location of precursors, adjusting the appropriate growing temperature and time, and establishing proper ventilation. Experimental results show the successful growth of a large-area single-layer MoS_2 on a sapphire substrate through direct sulfurization under a suitable environment. The thickness of the MoS_2 film determined by AFM measurement is about 0.73 nm. The peak difference between the Raman measurement shift of 386 and 405 cm^{-1} is 19.1 cm^{-1}, and the peak of PL measurement is about 677 nm, which is converted into energy of 1.83 eV, which is the size of the direct energy gap of the MoS_2 thin film. The results verify the distribution of the number of grown layers. Based on the observation of the optical microscope (OM) images, MoS_2 continuously grows from a single layer of discretely distributed triangular single-crystal grains into a single-layer large-area MoS_2 film. This work provides a reference for growing MoS_2 in a large area. We expect to apply this structure to various heterojunctions, sensors, solar cells, and thin-film transistors.

Two-dimensional layered material MoS_2 with atomically thick layers is one of the most common transition metal dichalcogenides (TMDs)[1–4]; it has an indirect energy gap of 1.2 eV in the bulk MoS_2 semiconductor and a direct energy gap of 1.8 eV in the monolayer MoS_2[5–9]. Single-layer TMDs has an excellent current switch ratio (on/off current ratio) in field effect transistors because of its direct energy gap[10,11]. These advantages can only be possessed by materials with atomic thickness[12]. MoS_2 is a layered structure, which has good lubricity, pressure resistance, and wear resistance. It is mostly used in solid lubricants as well as in high-speed, heavy-duty, high-temperature, and chemical corrosion conditions[13–17]. This material has many potential applications, such as in field effect transistors, electronic devices, light-emitting diodes, sensors, and so on, due to its excellent optoelectronic properties[11,18–25]. In recent years, it has been found that MoS_2 has semiconductor properties and can exist in the form of a single layer or a few layers[26]. Therefore, two-dimensional materials are widely discussed and studied by scientists. Many methods, including mechanical exfoliation[12,27–30], thermally decomposed ammonium thiomolybdate[31–34], sulfurization of Mo/MoO_3[35], and chemical vapor deposition (CVD)[36–42], can be used to synthesize continuous MoS_2 films. These methods are capable of producing many good quality MoS_2 layers, however, achieving large area MoS_2 thin films is challenging. The reason is that MoS_2 tends to transform into nanoparticle and nanotube structures, leading to inefficient production in homogeneous synthesis and large-area MoS_2 thin films, making it challenging to deploy production for electronic devices. Therefore, synthesizing large-area MoS_2 thin films has attracted much research attention.

The growing method of this study is the direct sulfidation using molydenum/molybdenum oxide which also proposed by Lin et al.[35] in 2012. The main process is to perform direct sulfurization reaction on a substrate coated with molybdenum oxide to obtain a MoS_2 thin film. Molybdenum trioxide (MoO_3) of about 3.6 nm is plated

[1]Division of Gastroenterology, Department of Internal Medicine, Kaohsiung Armed Forces General Hospital, 2, Zhongzheng 1st.Rd., Lingya District, Kaohsiung City 80284, Taiwan. [2]Department of Mechanical Engineering, National Chung Cheng University, 168, University Rd., Min Hsiung, Chia Yi 62102, Taiwan. [3]Nikolaev Institute of Inorganic Chemistry, Siberian Branch of Russian Academy of Sciences, Novosibirsk, Russia 630090. [4]Department of Natural Sciences, Novosibirsk State University, 1, Pirogova Str., Novosibirsk, Russia 630090. [5]Department of Nursing, Tajen University, 20, Weixin Rd., Yanpu Township 90741, Pingtung County, Taiwan. [6]Director of Technology Development, Hitspectra Intelligent Technology Co., Ltd., 4F., No. 2, Fuxing 4th Rd., Qianzhen Dist., Kaohsiung City 80661, Taiwan. ✉email: forevershiningfy@yahoo.com.tw; hcwang@ccu.edu.tw

on a sapphire substrate and grown through two stages of heating. In the first stage, the heating time is one hour. The sample is placed into a furnace tube at 500 °C and passed through Ar/H_2 mixed gas ($Ar:H_2 = 4:1$) under controlled pressure of 1 Torr to convert MoO_3 into MoS_2. The reaction equation is as follows:

$$MoO_3(s) + H_2(g) \rightarrow MoO_2 + H_2O(g), \quad (1)$$

In the second stage, the heating time is 30 min. Sulfur powder is placed into a tube first, and Ar/H_2 mixed gas is introduced at 1000 °C. The pressure is controlled at 600 Torr. The MoO_2 in the first stage reacts with sulfur vapor inside the tube to form MoS_2. The reaction equation is as follows:

$$MoO_2(s) + 2S(g) \rightarrow MoS_2(s) + O_2(g), \quad (2)$$

The advantage of the direct sulfurization of molybdenum oxide is that it can grow a large area of MoS_2 film and is similar to two-stage thermal decomposition.

In 2014, Choudhary et al.[43] ref proposed a large-scale synthesis of MoS_2 on a Si/SiO_2 substrate using a two-step sputtering CVD method. The first step involved the deposition of Mo thin films on the substrate through the sputtering of Mo metal. In the second step, low-pressure CVD was employed to synthesize MoS_2. Argon gas was used to transport sulfur into the reactor, where it reacted with the Mo film. Upon annealing at a high temperature of 600 °C and subsequent cooling to room temperature, the Mo films were successfully converted to MoS_2 films. The results showed that this method effectively enabled the synthesis of large-area MoS_2 from Mo thin films, and the thickness of the synthesized MoS_2 films could be modulated by varying the sputtering times. The aforementioned studies indicate that large-area MoS_2 thin films can be synthesized using a CVD process. This involves exposing a thin film containing Mo to sulfur powder in an Argon gas environment and subjecting the sample to high temperature conditions. The results demonstrate that this approach can yield MoS_2 thin films with a substantial surface area.

In this study, we present the synthesis of MoS_2 thin films through a CVD process. Our findings indicate that a Mo thin film can be converted into a MoS_2 thin film using this method. Raman mapping, AFM, and high-resolution transmission electron microscopy (HRTEM) images confirmed the presence of a monolayer on the 2-inch sapphire wafer. Compared with MoS_2 films grown on Si substrates, electrical measurements of sapphire substrates growth revealed p-type semiconducting behavior with remarkably high electron mobility and on–off ratio. This approach is compatible with conventional semiconductor processes and can be extended to other TMDs and arbitrary substrates by transferring MoS_2.

Materials and Methods

Experimental materials and drug specifications of MoS_2. A double-side polished sapphire substrate with a thickness of 300 nm was utilized for the growth of MoS_2. The substrate was pre-coated with a 5 Å MoO_3 film through sputter deposition. Subsequently, direct sulfidation was performed using sulfur powder (S) of 99.98% purity. The purpose is to avoid impurity residues that affect chemical vapor deposition or single-crystal residue impurities. The quartz tube and ceramic crucible in the high-temperature furnace tube (Tubular thermal) are cleaned with aqua regia. The concentrations of nitric acid and hydrochloric acid in aqua regia are 37% and 68–69%, respectively, to avoid impurities from the previous growth remaining in the cleaning process.

Process and steps of growing MoS_2 by direct sulfurization. The process of this study is shown in Fig. 1, a 2-inch sapphire substrate with 300 nm thickness pre-deposited 5 Å MoO_3 was first prepared, cut into four equal parts, and cleaned with ultrasonic vibration in acetone for 10 min to remove surface impurities and oil stains and achieve a clean surface. Deionized water was used to remove organic solvent-acetone in ultrasonic vibration for 10 min. The sample was collected, and a high-pressure nitrogen gun was used to remove the moisture on the surface of the substrate. Direct sulfurization was used to grow MoS_2. The substrate was placed under specific pressure and temperature conditions. In the furnace tube system, argon was used as the carrier gas to perform chemical reactions on the surface of the substrate by hot steam vulcanization to generate high-quality, large-area films. The application of direct sulfurization method in the preparation of single-layer TMDs started with the growth of MoS_2. Initially, 500 sccm of argon gas was introduced to clean the interior of the system. The cavity was kept in a clean environment, and excess water vapor and oxygen in the quartz tube were removed for 10 min. The sample was grown with an argon flow rate of 400 sccm at a heating rate of 30 °C per minute. The growth temperature was 750 °C, which was maintained for 5 min. After the growth was completed, the gas volume was slowly decreased to − 40 sccm per minute to reduce the damage of the newly formed MoS_2 by airflow. The cover was opened once the temperature decreased to 400 °C. After opening the cover, the temperature was reduced to room temperature, and MoS_2 structure was obtained at high temperatures. A 1/4 two-inch sapphire substrate with 1.2 g of sulfur powder (S) as a precursor was placed on a crucible in a furnace tube. The vaporization point of Mo is above 650 °C and the vaporization point of S is above 200 °C; as such, Mo in the gaseous phase under a high-temperature environment will undergo a chemical reaction to produce molybdenum oxide (MoO_{3-x}) intermediate. The produced molybdenum oxide intermediate will diffuse to the substrate and react with vaporized sulfur to form MoS_2 film. The distance between the substrate and sulfur layer is 24 cm. The single-layer large-area MoS_2 can be effectively prepared by direct sulfurization. This method not only grows high-quality single-crystal materials but also prepares a large-area uniformly distributed film, which is beneficial to subsequent optoelectronic component manufacturing.

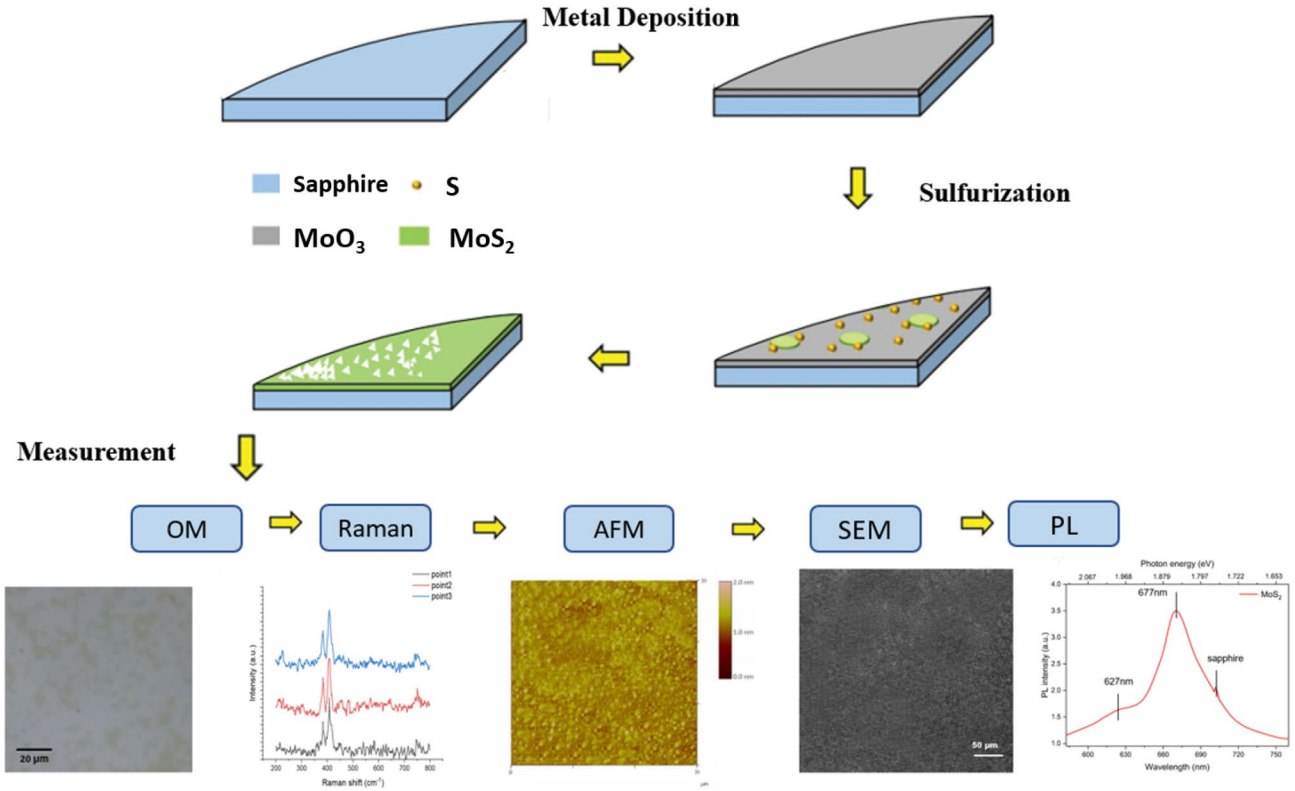

Figure 1. The flow chart of this study, starting with the growth of the material, followed by the optical measurement, and finally the measurement and analysis of the material properties.

Results

Optical microscope analysis. Under the optical microscope, the growth types of MoS_2 have different shape distributions on the substrate. Figure 2 shows the optical microscope (OM) of MoS_2 grown on the sapphire substrate. Figure 2a shows the substrate after actual growth, where the blue arrow indicates the direction of argon gas flow during CVD. The positions b, c, d, and e in the image present the growth distributions of different MoS_2 shapes; Fig. 2b shows the OM image at position b in Fig. 2a, in which we found a single layer of MoS_2 grown on the substrate in a large area, covering a larger area and almost completely covering the sapphire substrate. Figure 2c shows the OM image at position c in Fig. 2a, where the growth of single-layer MoS_2 is not as good as that at position b, but single-layer MoS_2 covers a larger area. Figure 2d shows the OM image at position d in Fig. 2a, in which the monolayer MoS_2 grows irregularly on the sapphire substrate and has a light blue irregular shape distribution, indicating the existence of monolayer MoS_2. Figure 2e is the OM image at position e in Fig. 2a, where the gray area is the sapphire substrate, and the scattered blue area is the area where MoS_2 grows.

SEM analysis. We analyzed the growth of single-layer MoS_2 thin film. Figure 3 shows the SEM image of junction between large area MoS_2 and scattered MoS_2 grown on the sapphire substrate. The size of MoS_2 in the scattered area is about 20–30 μm. In the OM image, we can see uniform triangular or star-shaped two-dimensional structured MoS_2 (Fig. 4a). Figure 4b shows a MoS_2 SEM image that is single-layer and complete triangular. Taking a triangle as an example, Fig. 4c shows the SEM image of a large-area MoS_2 thin film.

Raman spectroscopy analysis. We performed Raman measurement on the sapphire substrate sample grown with MoS_2. A laser with a wavelength of 532 nm was used as the excitation light source. The X-axis in the spectrum represents the Raman shift, and the Y-axis represents the Raman intensity. Figure 5a shows the Raman measurement map of the scattered MoS_2 in the region e of the OM image of MoS_2 in Fig. 2a. We take the black, red, and blue points inside to measure the large-area growth as shown in Fig. 5b. Figure 5c shows the Raman measurement map of large-area MoS_2 corresponding to the three black, red, and blue points in Fig. 5b.

The Raman shift is between 386.2 and 405.3 cm^{-1}, and the value of peak difference (Δk) is about 19.1 cm^{-1}. The results show that the large-area growth regions are all monolayers. Figure 5d shows the selected OM image of the Raman mapping range. Figure 5e presents the out-of-plane (A_{1g}) Raman mapping image of Fig. 5d. The sapphire substrate is identified as the green portion. The distribution of single-layer MoS_2 exhibits a relatively flat profile ranging from light green to yellow, and progressing towards orange-red on the graph. The mapping size of 50 μm × 50 μm shows a limited sampling area, yet the distribution remains consistently flat. This is further verified through Raman measurement, which demonstrates a uniform distribution of single-layer MoS_2. These findings highlight the potential of MoS_2 as a suitable material for the production of semiconductor devices.

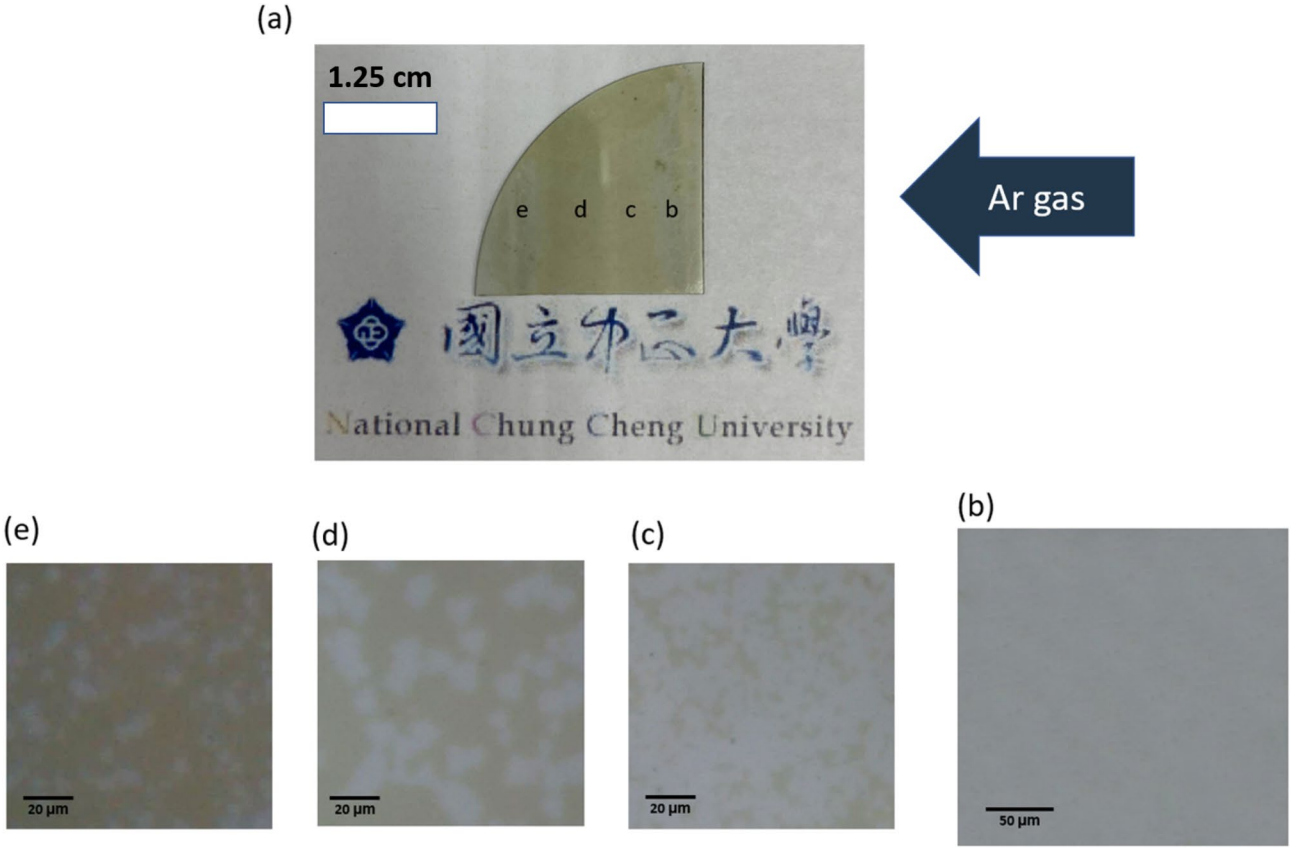

Figure 2. (**a**) Image of the sapphire substrate after the MoS_2 growth is completed, (**b**–**e**) The OM images at positions (**b**–**e**) correspond to the positions indicated on the substrate in (**a**).

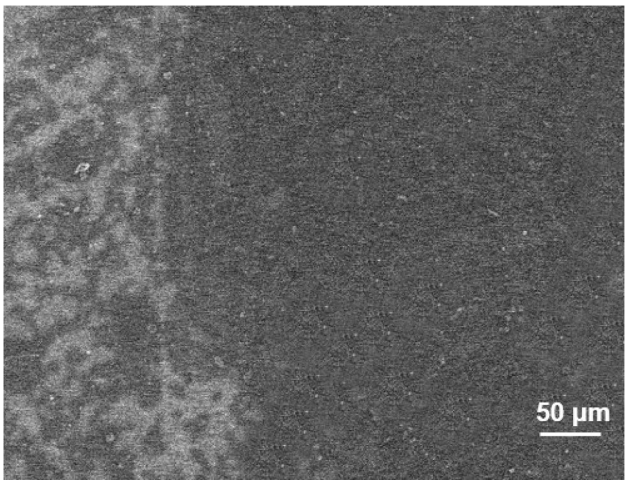

Figure 3. SEM image of junction between large area MoS_2 and scattered MoS_2 growth on sapphire substrate.

Atomic force microscopy analysis. The thickness of the MoS_2 thin film was determined through AFM measurement. The surface morphology and height profile results are shown in Fig. 6a,b, respectively. In Fig. 6a, the surface of the sapphire substrate and MoS_2 can be clearly seen. Figure 6b shows that the thickness of the grown MoS_2 on the sapphire substrate is 0.72 nm from the height profile of the cross-sectional line in Fig. 6a. This result indicates the successful synthesis of a single-layer MoS_2 structure. In Fig. 6b, there is no substantial difference in profile height between the MoS_2 layers or between the MoS_2 layer and the sapphire surface. The average roughness of MoS_2 films, as measured by AFM, ranges from 0.55 to 2.35 nm. It is important to note that AFM images depict the average distances of atoms on the sample surface, rather than the individual atoms themselves. In Fig. 6c, the 30 μm × 30 μm surface topography map of MoS_2 displays a relatively uniform distribution of

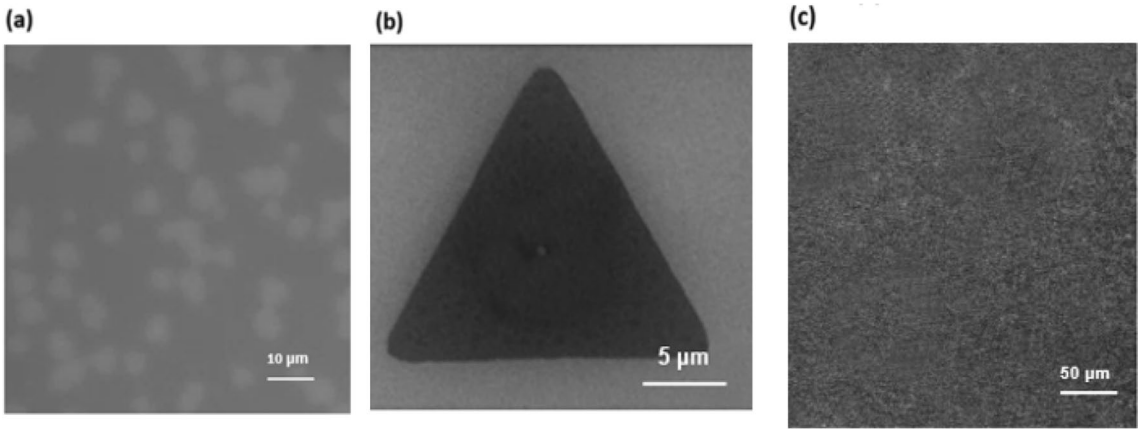

Figure 4. (**a**) OM and (**b**) SEM image of MoS_2 grown by direct sulfurization method (**c**) SEM images of large-area MoS_2 thin films in a large area.

molecules, as indicated by the color bar. However, a slight asymmetry in distribution is also observed, suggesting that the MoS_2 surface has a relatively smooth state.

PL spectral analysis. Figure 7 shows the PL emission spectrum of MoS_2. In the measurement, the 532 nm band was used as the laser excitation light source. The spectrum consists of two peaks, corresponding to A1 and B1 excitons at 677 and 627 nm, respectively. Both excitons have a direct excitonic transition from the valence band spin-orbital coupling energy separation[44]. The direct excitonic transition of the two resonances is the K point in the Brillouin zone. In general, the peak of MoS_2 luminescence is about 67 nm, and the converted energy is 1.86 eV, which is the size of the direct energy gap of the MoS_2 film. Based on the above data, the MoS_2 grown has a single-layer structure.

Discussions

In 2017, Zhu et al. reported the presence of two types of seed centers in the growth mechanism of MoS_2, namely: (1) molybdenum-oxysulfide (MoO_xS_{2-y}) nanoparticles or nanocrystals for growing multilayer MoS_2 and (2) two main edge-terminated irregular polygons for the growth of monolayer MoS_2, the S-Mo Klein edge and the Mo zigzag edge, which appear roughly in equal quantities[45]. The morphology then evolves into a nearly triangular shape with predominant Mo meandering edges. Using a CVD system to grow MoS_2, the impact of gas flow rate on MoS_2 growth can be studied. The Ar flow rate was varied between 200 and 500 sccm. Results show that a faster flow rate mainly produced single layers, while a slower flow rate resulted in more layers. When the deposition rate exceeds the growth rate of MoS_2, S-dominant growth occurs, which is the mechanism for monolayer MoS_2 growth. Conversely, when the deposition rate is slower than the growth rate of MoS_2, the dominant growth is molybdenum-oxysulfide, which is the mechanism for minority layer MoS_2 growth.

In 2018, Zhou et al. further investigated the seed crystals responsible for the two growth mechanisms and the impact of temperature, in addition to gas flow rate, on the deposition rate[46]. The study's experimental results revealed that temperature with a central nucleation point played a significant role in the formation of the seed crystals.

In the same time, Taheri et al. shown that a three-stage mechanism was proposed for the growth of MoS_2[47]. The first stage involves the evaporation of MoO_3, which may be facilitated by the presence of sulfur. This can either result in the partial reduction of MoO_3 to form MoS_2 or the creation of molybdenum oxysulfide, both of which are volatile in nature. The evaporated molybdenum oxide then diffuses to regions on the substrate with lower molybdenum concentrations, as a result of the chemical potential difference. The experimental results by Taheri et al. revealed that under the conditions used in their study, diffusion lengths can attain values in the tens of micrometers range. This process plays a role in mitigating local morphological changes at the nanoscale within the precursor MoO_3 films. In other words, the precursor film grows uniformly on the substrate as a local source of molybdenum, but does not dictate the ultimate morphology of the final MoS_2. The second stage entails sulfidation to produce MoS_2 through processes such as substitution of sulfur, lattice reorganization, and material redistribution. This leads to the uniform formation of single-crystal triangles of MoS_2 across the substrate. The third stage involves the growth and merging of these triangles to form continuous MoS_2. During this stage, MoS_2 nanoparticles evaporate and are redeposited along the edges of the discrete triangles. The high density of triangles and long diffusion length allow for easy merging of the triangles, resulting in the filling of any gaps and the formation of continuous triangles with minimal overgrowth and voids. Meanwhile, the nanoparticles undergo evaporation and are not consumed. Unlike the growth process of CVD, there are no specific nucleation sites that cause morphological changes in MoS_2. Instead, the process of vapor diffusion and nucleation under sulfidation occurs uniformly and locally at the microscale across the entire substrate, resulting in continuous MoS_2 coverage. A unique aspect of the synthesis process is the cessation of carrier gas flow during the cooling step. Although MoS_2 has a melting temperature of 1185 °C, its vapor pressure is small but not negligible at temperatures above 700 °C. By stopping the flow of the carrier gas, the trapped MoS_2 vapor remains in equilibrium with the grown

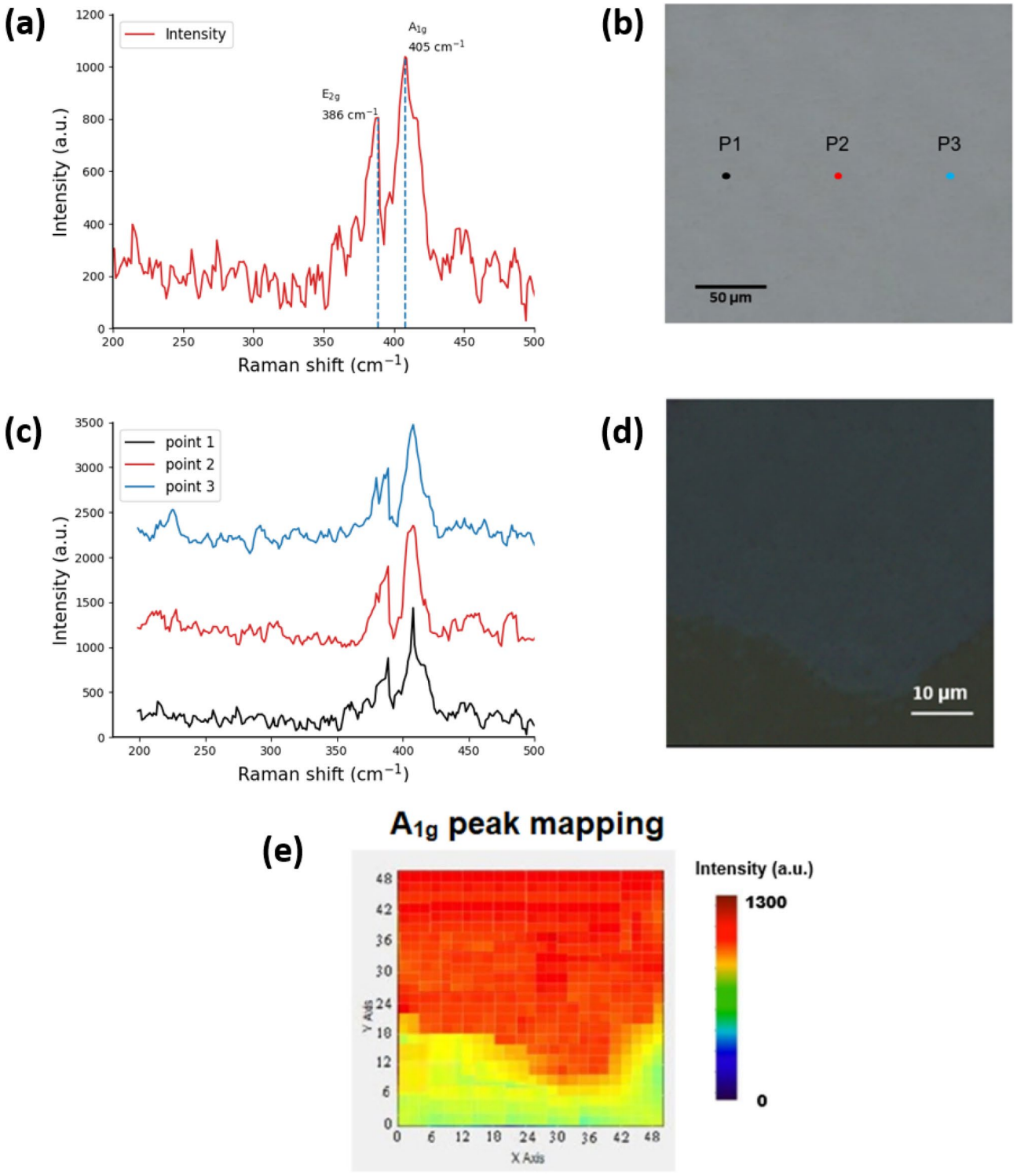

Figure 5. (**a**) Raman spectrum measurement map of a single layer (**b**) Raman spectrum measurement point schematic diagram (**c**) Raman spectrum measurement map of different selected areas (**d**) OM image of the selected Raman mapping range, (**e**) is the Raman mapping diagram of A_{1g}.

MoS_2 crystals on the substrate for a longer period, thus preventing further evaporation of the film. Controlled experiments conducted by Taheri et al. showed that partial retention of MoS_2 was achieved after annealing at 700 °C for 30 min in the presence of sulfur. Conversely, continuous air flow during cooling will cause the slow evaporation of MoS_2, leading to its gradual loss and resulting in the formation of discrete triangular islands. This was confirmed by the experiment where complete evaporation of MoS_2 was observed after only 5 min of annealing at 650 °C in the presence of nitrogen flow. These results strongly support the role of sulfur vapor in

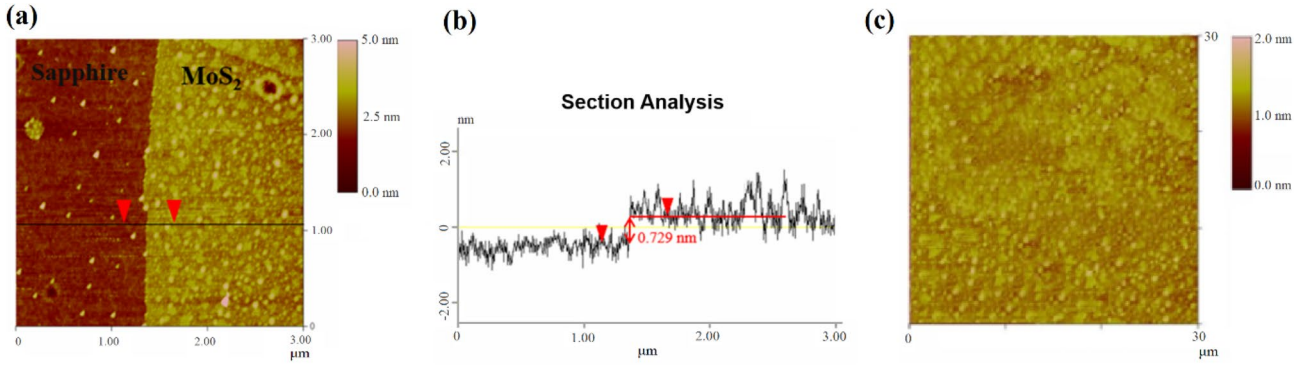

Figure 6. AFM image of MoS_2, (**a**) is the surface morphology of sapphire substrate and MoS_2, (**b**) is the height profile result of (**a**) cross-section, (**c**) is the surface morphology of large-area MoS_2.

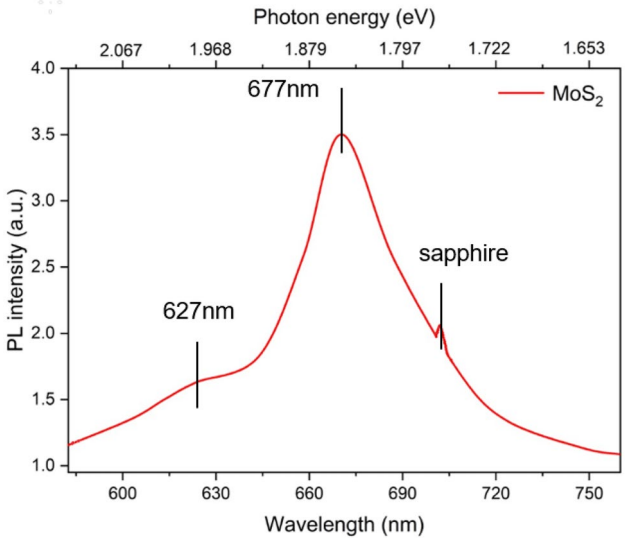

Figure 7. PL measurement results of monolayer MoS_2, the luminescence band is at 677 nm, and the conversion energy is 1.83 eV.

the growth of continuous MoS_2. According to the flow direction of Argon gas, the growth of MoS_2 progresses from a large coverage area to a smaller one, from fragmentation to large-area growth. By avoiding low-pressure growth, the process in a low-pressure environment minimizes unnecessary gas-phase reactions, which can lead to uneven distribution of gasified sulfur atoms. The resultant differences in the concentration of sulfur atoms can result in changes in the morphology of MoS_2 from fragmentation to a more uniform, large-area distribution.

The Raman spectroscopy measurement showed that the grown MoS_2 exhibits the characteristics of a monolayer. Raman mapping is the best method for analyzing the number of layers[48–50]. The PL spectral analysis results indicated that the distribution of the grown MoS_2 monolayer is uniform, as demonstrated by the mapping diagrams obtained with the excitation light peak at 627 nm or 677 nm. The thickness of the sapphire substrate with periodic growth of MoS_2 was analyzed using AFM. The selected area was confirmed to be a single layer, consistent with the results obtained from the Raman and PL spectroscopy analysis.

Conclusions

The research can be divided into two parts. In the first part, we refer to the relevant literature and successfully grow large-area MoS_2 in some areas of the sapphire substrate by changing the parameters through direct sulfurization. The single-layer thin film successfully overcomes the limitations of growing a large-area single-layer MoS_2 thin film in chemical vapor deposition. In addition to adjusting the parameters, the method can achieve a continuous thin film of about 500 μm × 500 μm. The second part is the analysis of the results of Raman spectroscopy, photoluminescence spectroscopy, atomic force microscopy, and scanning electron microscopy. The large-area MoS_2 film is composed of scattered triangular MoS_2. The MoS_2 film grown has monolayers. In summary, desirable modulated layers with a large area of MoS_2 can be achieved by growth techniques using sulfided pre-deposited transition metals through sequential transition metal deposition and direct sulfurization.

Future works should grow large-area single-layer MoS_2 thin films by direct sulfurization to develop MoS_2 thin film for field effect transistors. In the past, semiconductors used three-dimensional materials, and the physical properties and device structures were developed to the 3-nm node. The present research used two-dimensional materials, with thickness less than 1 nm (1–3 layers of atomic thickness), which is closer to the limit of the thickness of solid semiconductor materials. The monolayer disulfide has a direct energy gap, making it suitable for application to solar cells. Previous works also used this characteristic to make solar cells with p-type materials, but many studies are limited by the size of MoS_2 films. The present study contributes to knowledge on large-area growth to overcome existing problems and improve the efficiency performance of power generation.

Data availability

The datasets used and/or analyzed during the current study available from the corresponding author on reasonable request.

Received: 11 March 2023; Accepted: 20 May 2023
Published online: 24 May 2023

References

1. Zhang, Y., Wan, Q. & Yang, N. Recent advances of porous graphene: Synthesis, functionalization, and electrochemical applications. *Small* **15**(48), 1903780 (2019).
2. Yang, D. *et al.* Cut flexible multifunctional electronics using MoS_2 nanosheet. *Nanomaterials* **9**(7), 922 (2019).
3. Li, K.-C. *et al.* Intelligent identification of MoS_2 nanostructures with hyperspectral imaging by 3D-CNN. *Nanomaterials* **10**(6), 1161 (2020).
4. Mukundan, A., Tsao, Y.-M., Artemkina, S. B., Fedorov, V. E. & Wang, H.-C. Growth mechanism of periodic-structured MoS_2 by transmission electron microscopy. *Nanomaterials* **12**(1), 135 (2021).
5. Kashid, R. V. *et al.* Enhanced field-emission behavior of layered MoS_2 sheets. *Small* **9**(16), 2730–2734 (2013).
6. Wang, F. *et al.* Synthesis, properties and applications of 2D non-graphene materials. *Nanotechnology* **26**(29), 292001 (2015).
7. Schulman, D. S. *et al.* Facile electrochemical synthesis of 2D monolayers for high-performance thin-film transistors. *ACS Appl. Mater. Interfaces* **9**(51), 44617–44624 (2017).
8. He, Z. & Que, W. Molybdenum disulfide nanomaterials: Structures, properties, synthesis and recent progress on hydrogen evolution reaction. *Appl. Mater. Today* **3**, 23–56 (2016).
9. Ding, Q., Song, B., Xu, P. & Jin, S. Efficient electrocatalytic and photoelectrochemical hydrogen generation using MoS_2 and related compounds. *Chemistry* **1**(5), 699–726 (2016).
10. Radisavljevic, B., Radenovic, A., Brivio, J., Giacometti, V. & Kis, A. Single-layer MoS_2 transistors. *Nat. Nanotechnol.* **6**(3), 147–150 (2011).
11. Sarkar, D. *et al.* MoS_2 field-effect transistor for next-generation label-free biosensors. *ACS Nano* **8**(4), 3992–4003 (2014).
12. Wang, Q. H., Kalantar-Zadeh, K., Kis, A., Coleman, J. N. & Strano, M. S. Electronics and optoelectronics of two-dimensional transition metal dichalcogenides. *Nat. Nanotechnol.* **7**(11), 699–712 (2012).
13. Jo, G. *et al.* The application of graphene as electrodes in electrical and optical devices. *Nanotechnology* **23**(11), 112001 (2012).
14. Nguyen, B. H. & Nguyen, V. H. Promising applications of graphene and graphene-based nanostructures. *Adv. Nat. Sci. Nanosci. Nanotechnol.* **7**(2), 023002 (2016).
15. Singh, A. K. & Eom, J. Negative magnetoresistance in a vertical single-layer graphene spin valve at room temperature. *ACS Appl. Mater. Interfaces* **6**(4), 2493–2496 (2014).
16. Pang, S., Hernandez, Y., Feng, X. & Müllen, K. Graphene as transparent electrode material for organic electronics. *Adv. Mater.* **23**(25), 2779–2795 (2011).
17. Luo, L.-L. *et al.* First-principles calculations of 0D/2D GQDs–MoS_2 mixed van der Waals heterojunctions for photocatalysis: A transition from type I to type II. *Phys. Chem. Chem. Phys.* **24**(14), 8529–8536 (2022).
18. Yang, K., Liu, H., Wang, S., Li, W. & Han, T. A horizontal-gate monolayer MoS_2 transistor based on image force barrier reduction. *Nanomaterials* **9**(9), 1245 (2019).
19. Lu, G. Z. *et al.* Electrically pumped white-light-emitting diodes based on histidine-doped MoS_2 quantum dots. *Small* **15**(30), 1901908 (2019).
20. Lee, C.-H. *et al.* Atomically thin p–n junctions with van der Waals heterointerfaces. *Nat. Nanotechnol.* **9**(9), 676–681 (2014).
21. Zhao, J. *et al.* Highly sensitive MoS_2 humidity sensors array for noncontact sensation. *Adv. Mater.* **29**(34), 1702076 (2017).
22. Park, Y. J. *et al.* All MoS_2-based large area, skin-attachable active-matrix tactile sensor. *ACS Nano* **13**(3), 3023–3030 (2019).
23. Shin, M., Yoon, J., Yi, C., Lee, T. & Choi, J.-W. Flexible HIV-1 biosensor based on the Au/MoS_2 nanoparticles/Au nanolayer on the PET substrate. *Nanomaterials* **9**(8), 1076 (2019).
24. Tong, X., Ashalley, E., Lin, F., Li, H. & Wang, Z. M. Advances in MoS_2-based field effect transistors (FETs). *Nano-Micro Lett.* **7**(3), 203–218 (2015).
25. Jeong, S.-J. *et al.* Physisorbed-precursor-assisted atomic layer deposition of reliable ultrathin dielectric films on inert graphene surfaces for low-power electronics. *2D Materials* **3**(3), 035027 (2016).
26. Yin, Z. *et al.* Single-layer MoS_2 phototransistors. *ACS Nano* **6**(1), 74–80 (2012).
27. Bonaccorso, F. *et al.* Production and processing of graphene and 2d crystals. *Mater. Today* **15**(12), 564–589 (2012).
28. Wu, J. *et al.* Layer thinning and etching of mechanically exfoliated MoS_2 nanosheets by thermal annealing in air. *Small* **9**(19), 3314–3319 (2013).
29. Li, H., Wu, J., Yin, Z. & Zhang, H. Preparation and applications of mechanically exfoliated single-layer and multilayer MoS_2 and WSe_2 nanosheets. *Acc. Chem. Res.* **47**(4), 1067–1075 (2014).
30. Ottaviano, L. *et al.* Mechanical exfoliation and layer number identification of MoS_2 revisited. *2D Materials* **4**(4), 045013 (2017).
31. Liu, K.-K. *et al.* Growth of large-area and highly crystalline MoS_2 thin layers on insulating substrates. *Nano Lett.* **12**(3), 1538–1544 (2012).
32. Vinoba, M., Navvamani, R. & Al-Sheeha, H. Controllable thermal conversion of thiomolybdate to active few-layer MoS_2 on alumina for efficient hydrodesulfurization. *SN Appl. Sci.* **1**(4), 1–11 (2019).
33. Salam, A., Xie, G., Guo, D. & Xu, W. Fabrication and tribological behavior of self-lubricating composite impregnated with synthesized inorganic hollow fullerene-like MoS_2. *Compos. B Eng.* **200**, 108284 (2020).
34. Pazhamalai, P., Krishnamoorthy, K., Sahoo, S., Mariappan, V. K. & Kim, S.-J. Supercapacitive properties of amorphous MoS_3 and crystalline MoS_2 nanosheets in an organic electrolyte. *Inorg. Chem. Front.* **6**(9), 2387–2395 (2019).
35. Lin, Y.-C. *et al.* Wafer-scale MoS_2 thin layers prepared by MoO_3 sulfurization. *Nanoscale* **4**(20), 6637–6641 (2012).
36. Najmaei, S. *et al.* Vapour phase growth and grain boundary structure of molybdenum disulphide atomic layers. *Nat. Mater.* **12**(8), 754–759 (2013).

37. Wang, S. *et al.* Shape evolution of monolayer MoS_2 crystals grown by chemical vapor deposition. *Chem. Mater.* **26**(22), 6371–6379 (2014).
38. Kim, H., Ovchinnikov, D., Deiana, D., Unuchek, D. & Kis, A. Suppressing nucleation in metal–organic chemical vapor deposition of MoS_2 monolayers by alkali metal halides. *Nano Lett.* **17**(8), 5056–5063 (2017).
39. Qian, S. *et al.* Growth of continuous MoS_2 film with large grain size by chemical vapor deposition. *Mater. Sci. Semicond. Process.* **93**, 317–323 (2019).
40. Kataria, S. *et al.* Growth-induced strain in chemical vapor deposited monolayer MoS_2: Experimental and theoretical investigation. *Adv. Mater. Interfaces* **4**(17), 1700031 (2017).
41. Sohn, W. *et al.* Microscopic evidence of strong interactions between chemical vapor deposited 2D MoS_2 film and SiO_2 growth template. *Nano Converg.* **8**(1), 1–10 (2021).
42. Löchner, F. J. *et al.* Hybrid dielectric metasurfaces for enhancing second-harmonic generation in chemical vapor deposition grown MoS_2 monolayers. *ACS Photonics* **8**(1), 218–227 (2020).
43. Choudhary, N., Park, J., Hwang, J. Y. & Choi, W. Growth of large-scale and thickness-modulated MoS_2 nanosheets. *ACS Appl. Mater. Interfaces* **6**(23), 21215–21222 (2014).
44. Zhang, W. *et al.* High-gain phototransistors based on a CVD MoS_2 monolayer. *Adv. Mater.* **25**(25), 3456–3461 (2013).
45. Zhu, D. *et al.* Capture the growth kinetics of CVD growth of two-dimensional MoS_2. *NPJ 2D Mater. Appl.* **1**(1), 1–8 (2017).
46. Zhou, D. *et al.* Unveiling the growth mechanism of MoS_2 with chemical vapor deposition: From two-dimensional planar nucleation to self-seeding nucleation. *Cryst. Growth Des.* **18**(2), 1012–1019 (2018).
47. Taheri, P. *et al.* Growth mechanism of largescale MoS_2 monolayer by sulfurization of MoO_3 film. *Mater. Res. Express* **3**(7), 075009 (2016).
48. Hsieh, Y.-P. *et al.* Effect of catalyst morphology on the quality of CVD grown graphene. *J. Nanomater.* **2013**, 6–6 (2013).
49. Wang, H.-C. *et al.* Large-area few-layered graphene film determination by multispectral imaging microscopy. *Nanoscale* **7**(19), 9033–9039 (2015).
50. Lu, M.-Y., Wu, S.-C., Wang, H.-C. & Lu, M.-P. Time-evolution of the electrical characteristics of MoS_2 field-effect transistors after electron beam irradiation. *Phys. Chem. Chem. Phys.* **20**(14), 9038–9044 (2018).

Author contributions

Conceptualization, K.Y.Y., H.-T.N., and Y.-M.T.; methodology, H.-C.W.; software, Y.-M.T.; validation, Y.-M.T., S.B.A., and V.E.F.; formal analysis, C.-W.H., H.-C.W.; investigation, H.-T.N.; resources, S.B.A., and V.E.F.; data curation, K.Y.Y., H.-T.N., and Y.-M.T.; writing—original draft preparation, H.-T.N.; writing—review and editing, C.-W.H., H.-C.W.; visualization, C.-W.H., H.-C.W.; supervision, C.-W.H., H.-C.W.; project administration, C.-W.H., H.-C.W.; funding acquisition, C.-W.H., H.-C.W. All authors have read and agreed to the published version of the manuscript.

Funding

This research was supported by the National Science and Technology Council, The Republic of China under the Grants NSTC 111-2221-E-194-007. This work was financially/partially supported by the Kaohsiung Armed Forces General Hospital research project KAFGH_D_112032 in Taiwan.

Competing interests

The authors declare no competing interests.

Additional information

Correspondence and requests for materials should be addressed to C.-W.H. or H.-C.W.

Reprints and permissions information is available at www.nature.com/reprints.

Publisher's note Springer Nature remains neutral with regard to jurisdictional claims in published maps and institutional affiliations.